nature protocols

https://doi.org/10.1038/s41596-023-00844-5

Protocol

Acoustic tweezers for high-throughput single-cell analysis

In the format provided by the authors and unedited

Supplementary Information

Acoustic tweezers for high-throughput single-cell analysis

Shujie Yang[1], Joseph Rufo[1], Ruoyu Zhong[1], Joseph Rich[2], Zeyu Wang[1], Luke P. Lee[3,4,5*], and Tony Jun Huang[1*]

[1]Thomas Lord Department of Mechanical Engineering and Materials Science, Duke University, Durham, NC 27708, USA

[2]Department of Biomedical Engineering, Duke University, Durham, NC 27708, USA

[3]Renal Division and Division of Engineering in Medicine, Department of Medicine, Brigham and Women's Hospital, Harvard Medical School, Boston, MA 02115, USA

[4]Department of Bioengineering, Department of Electrical Engineering and Computer Science, University of California, Berkeley, Berkeley, CA 94720, USA

[5]Institute of Quantum Biophysics, Department of Biophysics, Sungkyunkwan University, Suwon, Korea

[*]Email: lplee@bwh.harvard.edu; tony.huang@duke.edu

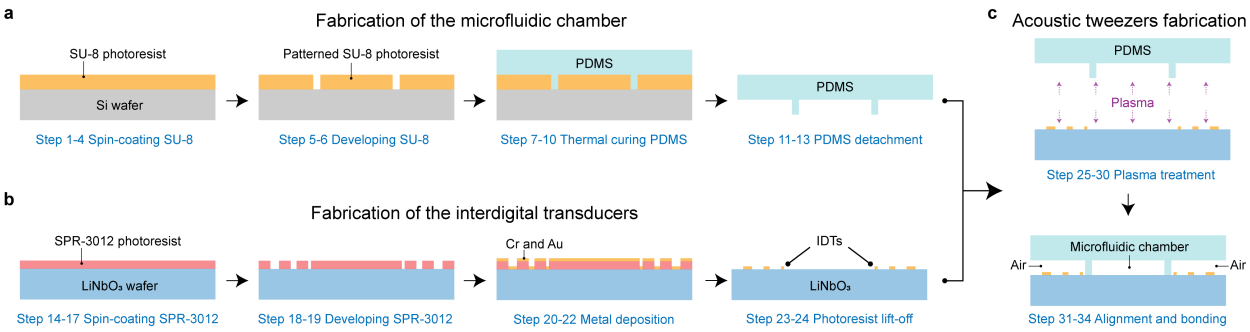

Supplementary Figure 1 | Fabrication of the acoustic tweezers. a, Schematic of the fabrication steps for the microfluidic chamber. **b,** Schematic of the fabrication steps for the interdigital transducers (IDTs) fabrication. **c,** Schematic of the device fabrication steps for the plasma treatment, alignment, and bonding.

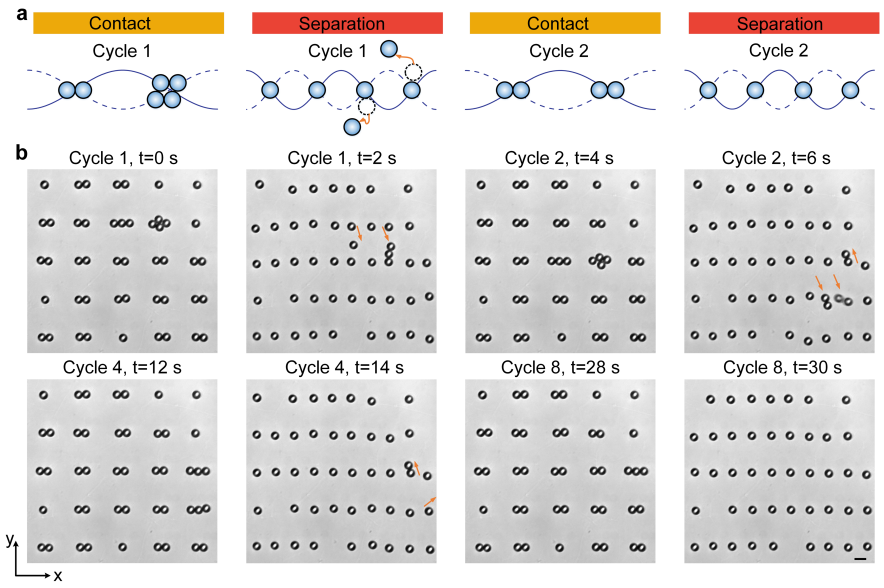

Supplementary Figure 2 | Enhancing particle pairing rate through a cyclic pairing-separation process. a, Schematics illustrating the process of enhancing the particle pairing rate *via* cyclic particle pairing and separation. Initially, as shown in cycle 1, particle clusters that include more than two particles were occasionally formed during the contact process. During the separation process, while applying the 2nd harmonic standing SAWs along the x-direction, the dimension of the acoustic wells was decreased, and only single particles could be trapped along the x-direction. As such, particle clusters will be disassembled by decreasing the size of the acoustic wells, and the undesired redundant particles will migrate and be trapped in nearby empty acoustic wells. **b**, Experimental results show that the particle pairing rate increased from 68% to 76% after 8 pairing-separation cycles over 30 s. Scale bar: 10 μm.

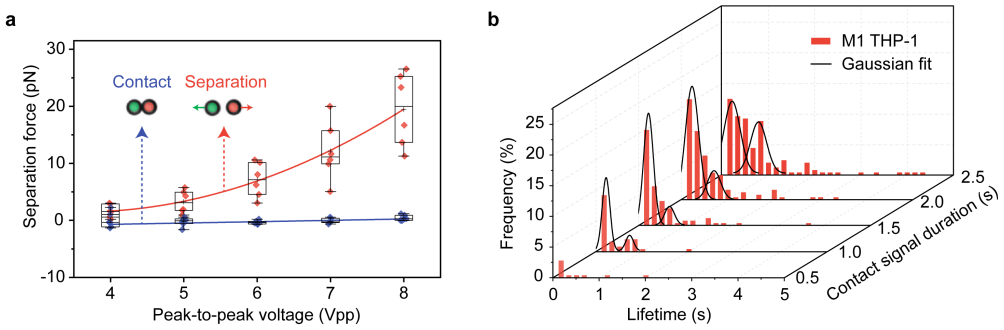

Supplementary Figure 3 | Anticipated results with the acoustic tweezers. a, Measured separation forces[34] (averaged from 6 particles) for pairing and separating the colloidal particles with various excitation signal amplitudes ranging from 4 to 8 V_{pp}. Data values of the minimum, lower quartile (25th percentile), median, upper quartile (75th percentile) and maximum are shown in the box plots. **b,** Histograms of cell adhesion lifetimes[34] for M1 THP-1 cells were obtained with different contact signal durations from 0.5 s to 2.5 s with an interval of 0.5 s. For each contact signal duration, 5 cell pairs were tested repeatedly over 50 contact cycles per pair to calculate the adhesion lifetime.

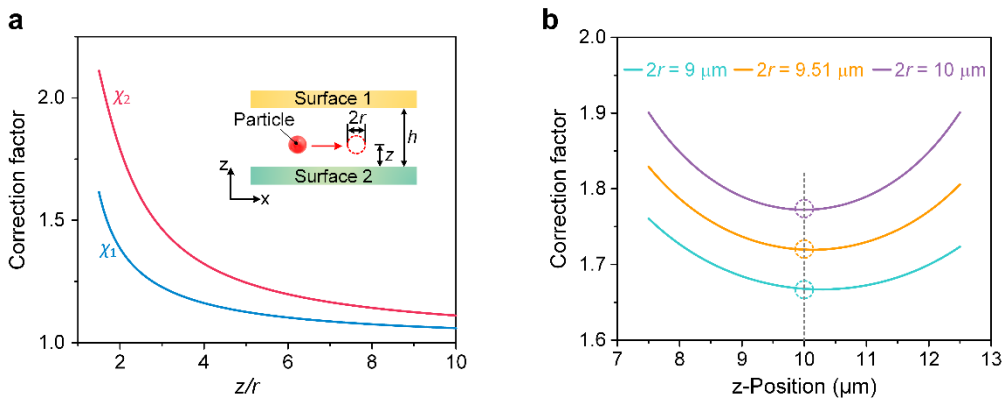

Supplementary Figure 4 | Correction of Stokes drag force for a single particle between two parallel surfaces[34]. a, Correction factors χ_1 (single surface) and χ_2 (two surfaces) as functions of *z*/*r*. **b,** Correction factor χ_2 as a function of particle positions along the z-direction for particles with different diameters (dashed circles).

Supplementary Table 1 | Key features of common piezoelectric materials.

Material	Transparency	Electromechanical coupling factor (K^2)	Surface acoustic wave generation	Price
PZT	No	23	No	$ 10 (2” disk)
AlN	Yes	6.5	Yes	$ 65 (2” wafer)
ZnO	Yes	8.5	Yes	$ 400 (0.4” wafer)
$LiTaO_3$	Yes	1.52	Yes	$ 316 (4” wafer)
GaAs	Yes	0.07	Yes	$ 152 (4” wafer)
Quartz	Yes	0.16	Yes	$ 50 (4” wafer)
128° Y-cut $LiNbO_3$	Yes	5.31	Yes	$ 68 (4” wafer)

Supplementary Note 1. Limitations of current acoustic tweezers

- **Limitation on the size range of trapping particles.** The spatial resolution of acoustic tweezers is determined by the wavelength of applied surface acoustic waves, mostly in micrometer scale. Current acoustic tweezers have been demonstrated to manipulate particles with sizes ranging from 100 nm to 10 mm[20]; however, manipulation of the individual nanoparticles that are smaller than 100 nm is still limited. Therefore, more exquisite acoustic tweezers that can generate nanometer-scale acoustic wavelength are required to increase the spatial resolution for more effective single nanoparticle manipulation.
- **Limitation on physical properties of trapping particles.** In addition to the particle size, other physical properties, such as the acoustic contrast factor, may limit the trapping capability of acoustic tweezers. The acoustic contrast factor is determined by the mass density and compressibility of both the particle and fluid. As shown in equations S1 and S2 in **Supplementary Note 2**, the acoustic radiation force is proportional to the acoustic contrast factor, and particles with larger acoustic contrast factor (larger density or smaller compressibility), such as gold nanoparticles, can be more easily manipulated in fluid. At the same time, biological nanoparticles with smaller acoustic contrast factors may have limited efficiency in acoustic manipulation due to trivial acoustic radiation forces[16,20,24].
- **Physical limitation on trapping smaller biological entities**. Acoustic streaming is the principal restriction on the effective manipulation of smaller (<1 μm) particles[24]. Fortunately, acoustic streaming is highly dependent on the device geometry, and innovative acoustic devices with dominant acoustic radiation force and negligible acoustic streaming-induced drag force can be achieved. For example, by modulating the applied acoustic waves, the recently developed wave-pillar excitation resonance method[64] can efficiently manipulate biological nanoparticles (<100 nm) with tunable cut-off sizes. Therefore, it is possible that the trapping and manipulation of small biological entities (larger than 50 nm), such as bacteria and viruses, can be conducted with acoustic tweezers.
- **Limitation on trapping asymmetric objects**. Acoustic tweezers have been well-characterized by trapping symmetric objects, such as polystyrene particles and cells. However, the manipulation of asymmetric objects, especially the alignment of asymmetric objects in their longitudinal or transverse directions, is quite limited because of the difficulty in controlling the shape of the acoustic trapping wells. Fortunately, the development of the novel acoustic tweezers enables more flexibility in modulating the shape of acoustic wells by applying time-effective Fourier-synthesized acoustic waves[34]. With the improvement of spatial resolution and novel design and operation methods, we believe that acoustic tweezers will successfully trap asymmetric objects, such as single erythrocyte, bacteria, and viruses, to study their interactions.

Supplementary Note 2: Force analysis of single particles and cells

As shown in equations S1 and S2, the acoustic radiation force $F_{\mathrm{a}}^{\mathrm{x}}$ generated in a one-dimensional sinusoidal standing wave is mainly determined by (1) particle parameters such as volume V_p, density ρ_p, and compressibility β_p; (2) wavelength (λ) of the applied surface acoustic wave (SAW); and (3) acoustic pressure p_0 that is determined by the amplitude of the applied excitation, electromechanical coupling coefficient K^2 of the piezoelectric substrate, finger-pairs of electrodes and even the design configuration of an IDT[34].

$$F_{\mathrm{a}}^{\mathrm{x}} = -\frac{\pi p_0^2 V_{\mathrm{p}} \beta_{\mathrm{f}}}{2\lambda} \varphi(\beta, \rho) \sin(2kx), \tag{S1}$$

$$\varphi(\beta, \rho) = \frac{5\rho_{\mathrm{p}} - 2\rho_{\mathrm{f}}}{2\rho_{\mathrm{p}} + \rho_{\mathrm{f}}} - \frac{\beta_{\mathrm{p}}}{\beta_{\mathrm{f}}}, \tag{S2}$$

where ρ_{f} is the fluidic density and β_{f} is the compressibility of the medium.

As a particle moves in a still fluid near a flat surface, the hydrodynamic interaction between the particle and the fluid is modified by the presence of the nearby surface, resulting in an increase in the Stokes drag force acting on the particle[65]. Thus, the Stokes drag force can be expressed as

$$\boldsymbol{F}_{\mathbf{d}}' = -6\pi\mu r \boldsymbol{v}_{\boldsymbol{r}} \chi, \tag{S3}$$

where μ is the fluid viscosity, r is the radius of a single spherical particle, $\boldsymbol{v}_{\mathrm{r}}$ is the particle velocity, and χ is the correction factor due to parallel translation along surfaces.

Faxén's correction[65] suggests that the correction factor χ for a particle moving parallel to a surface can be expressed using power series expansions up to fifth order:

$$\chi_1 = \frac{1}{1 - \frac{9}{16}\left(\frac{r}{z}\right) + \frac{1}{8}\left(\frac{r}{z}\right)^3 - \frac{45}{256}\left(\frac{r}{z}\right)^4 - \frac{1}{16}\left(\frac{r}{z}\right)^5}, \tag{S4}$$

where z is the distance between the particle and a surface. The linear superposition approximation method[74] is employed to compute the correction factor χ_2 for the scenario where two surfaces are present along the z-direction (**Supplementary Figure 4a**). The correction factor χ_2 can be expressed as:

$$\chi_2 = \chi_1(z) + \chi_1(h - z) - 1, \tag{S5}$$

where h is the distance between two surfaces.

One can calculate the correction factor χ_2 for different z-positions by applying equation (S4) to (S5). As depicted in **Supplementary Figure 4b**, the correction factor χ_2 reaches its minimum value when the particle is positioned near the middle plane and increases as the particle moves closer to either of the surfaces. According to our previous investigation[34], it is sufficient to calculate the correction factor associated with the

chamber height to correct the error in the Stokes drag force of a single particle in a microfluidic chamber with dimensions of $400 \times 400 \times 20$ μm^3.

The equation for the particle's momentum can be expressed as:

$$m\frac{d\boldsymbol{v}_{\mathrm{r}}}{dt} = \boldsymbol{F}_{\mathrm{r}} + \boldsymbol{F}'_{\mathbf{d}}, \tag{S6}$$

where m is the mass of the particle. One can describe the acoustic radiation force in the acoustic tweezers by substituting the corrected Stokes drag force equation (S3) into equation (S6):

$$\boldsymbol{F}_{\mathrm{r}} = \frac{4\pi r^3 \rho_{\mathrm{p}}}{3}\frac{d\boldsymbol{v}_{\mathrm{r}}}{dt} + 6\pi\mu r\boldsymbol{v}_{\boldsymbol{r}}\chi_2. \tag{S7}$$

The values of $r = 4.76\ \mu\mathrm{m}$ and $\rho_{\mathrm{p}} = 1060\ \mathrm{kg/m^3}$ correspond to the diameter and density, respectively, of the non-functionalized polystyrene beads. Therefore, with the velocity measured from a recorded video for particle position tracking, we can not only determine the acoustic radiation force using equation (S7), but also calculate the separation and contact forces. Either the separation force that is generated by applying a 2nd harmonic standing SAW or the contact force that is induced by the base standing SAW can be calculated through Newton's second law:

$$\boldsymbol{F}_{\mathrm{net}} = \rho_{\mathrm{p}}\frac{4\pi r^3}{3}\frac{d\boldsymbol{v}_{\mathrm{r}}}{dt}. \tag{S8}$$

For a more detailed calculation of the force, please refer to our previous studies[34].

References

74. Lin, B., Yu, J. & Rice, S.A. Direct measurements of constrained Brownian motion of an isolated sphere between two walls. *Phys. Rev. E* **62**, 3909 (2000).

Appendix

Appendix 1 | List of foundries for microfluidic mould and SAW device fabrication.

Fabrication services	Foundries	Links
Microfluidic mould	FlowJEM	www.flowjem.com
	SU8 Masters	www.su8masters.com
SAW devices	Angstrom Engineering	https://substratasolutions.com
	Deposition Technology Innovations	https://www.dtifilms.com
	Newlight Photonics	https://www.newlightphotonics.com